ELSEVIER

NeuroImage

www.elsevier.com/locate/ynimg
NeuroImage 32 (2006) 195 – 207

Mapping single-trial EEG records on the cortical surface through a spatiotemporal modality

Arthur C. Tsai,[a,*] Michelle Liou,[a] Tzyy-Ping Jung,[b] Julie A. Onton,[b] Philip E. Cheng,[a] Chien-Chih Huang,[a] Jeng-Ren Duann,[b] and Scott Makeig[b]

[a]*Institute of Statistical Science, Academia Sinica, Taipei 115, Taiwan*
[b]*Computational Neurobiology Laboratory, and Institute for Neural Computation, University of California, San Diego, CA 92093, USA*

Received 6 September 2005; revised 10 February 2006; accepted 27 February 2006
Available online 26 May 2006

Event-related potentials (ERPs) induced by visual perception and cognitive tasks have been extensively studied in neuropsychological experiments. ERP activities time-locked to stimulus presentation and task performance are often observed separately at individual scalp channels based on averaged time series across epochs and experimental subjects. An analysis using averaged EEG dynamics could discount information regarding interdependency between ongoing EEG and salient ERP features. Advanced tools such as independent component analysis (ICA) have been developed for decomposing collections of single-trial EEG records into separate features. Those features (or independent components) can then be mapped onto the cortical surface using source localization algorithms to visualize brain activation maps and to study between-subject consistency. In this study, we propose a statistical framework for estimating the time course of spatiotemporally independent EEG components simultaneously with their cortical distributions. Within this framework, we implemented Bayesian spatiotemporal analysis for imaging the sources of EEG features on the cortical surface. The framework allows researchers to include prior knowledge regarding spatial locations as well as spatiotemporal independence of different EEG sources. The use of the Electromagnetic Spatiotemporal ICA (EMSICA) method is illustrated by mapping event-related EEG dynamics induced by events in a visual two-back continuous performance task. The proposed method successfully identified several interesting components with plausible corresponding cortical activation topographies, including processes contributing to the late positive complex (LPC) located in central parietal, frontal midline, and anterior cingulate cortex, to atypical mu rhythms associated with the precentral gyrus, and to the central posterior alpha activity in the precuneus.

Keywords: Event-related potentials; ICA; Bayesian spatiotemporal analysis; Inverse problem

Introduction

For several decades, researchers have proposed techniques for localizing neural generators of event-related potentials (ERPs) associated with visual and other stimuli presented during performing EEG tasks (Scherg and Cramon, 1986; Liu et al., 1998; Baillet et al., 2001a). Because of the presence of instrumental and background noise as well as large inherent dynamic variability, ERPs are normally averaged across subjects and experimental trials before estimating their cortical origins both to increase the signal/noise ratio and, at the same time, to reduce the effects of non-neural artifacts (e.g., Tendolkar et al., 2000; Spencer et al., 2001; Halgren et al., 2002; Liu et al., 2003). However, averaged ERPs may filter out information regarding interdependency between ongoing EEG processes and salient ERP features. It has been shown that collections of single EEG trials can be decomposed into separate components using linear decomposition methods including principal component analysis (PCA) and independent component analysis (ICA, Makeig et al., 1996, 2002). The scalp maps associated with ERP-related EEG components can then be input into a source localization algorithm to estimate their EEG cortical sources. Identification of sources using ICA (at stage I), followed by estimation of their cortical locations (stage II), allows elimination of instrumental and physiological artifacts (Jung et al., 2000, 2001). This two-stage procedure has been claimed to yield more precise estimation of pointwise equivalent dipole source locations (e.g., Vigário et al., 1999; Tang et al., 2000; Zhukov et al., 2000; Cao et al., 2001).

In contrast to the above two-stage procedure, some researchers have attempted to localize equivalent dipole sources by simultaneously estimating their orientations and locations as well as time courses. For example using a time-varying equivalent dipole model, multi-channel ERPs were modeled as a summand of projections from a set of equivalent dipoles with fixed orientations and locations, yet time-varying amplitudes and polarities (Scherg and Cramon, 1985, 1986). This algorithm was implemented under the assumption that the number of sources was known or could be

* Corresponding author.
E-mail address: arthur@stat.sinica.edu.tw (A.C. Tsai).
Available online on ScienceDirect (www.sciencedirect.com).

1053-8119/$ - see front matter © 2006 Elsevier Inc. All rights reserved.
doi:10.1016/j.neuroimage.2006.02.044

estimated from singular-value decomposition. The MUSIC/RAP-MUSIC algorithm by Mosher et al. (1992) and Mosher and Leahy (1998) was a more computationally efficient approach that built an equivalent dipole source model using a PCA subspace projection. The two approaches were strongly dependent on the second-order statistics of the spatiotemporal EEG data averages.

While equivalent dipole models are ideal for modeling point sources, they may perform poorly for estimating neural sources distributed across one or more cortical regions, for instance, those sources induced by high-level cognitive processes (Nunez et al., 1991, 1994; Kincses et al., 1999). It is desirable to develop strategies for estimating current density sources that accommodate the source distributions rather than a skeleton of discrete equivalent cortical dipoles. Accordingly, minimum-norm estimators have been proposed that determine distributed cortical source regions with reasonable configurations (Hämäläinen and Ilmoniemi, 1984, 1994; Dale and Sereno, 1993). Because of computational simplicity, these estimators have been widely adopted in empirical studies (Liu et al., 1998; Moores et al., 2003; Fuchs et al., 1999). The approach of Schmidt et al. (1999), on the other hand, directly generalizes multiple dipole models to distributed current density models by constructing and sampling from a posterior distribution using Markov Chain Monte Carlo methods; the method performs Bayesian source density estimation of the distributions of unknown parameters with regard to the number, location, and extent of source regions.

There is a broad consensus that the average ERPs recorded during cognitive tasks are generated by multiple distributed sources (Moores et al., 2003). Empirical studies have also found that time courses of ERP features (e.g., the early visual N1 peak with following alpha ringing) vary across scalp locations, consistent with previous observations of multiple alpha rhythm sources with overlapping scalp and brain topographies (Andrew and Pfurtscheller, 1997; Lutzenberger, 1997; Makeig et al., 1999, 2002; Mangun, 1992). Therefore, equivalent dipole sources or current density models that avoid decomposing ERP records into subcomponents may not yield precise and spatially overlapping generators.

In this study, a spatiotemporal algorithm, Electromagnetic Spatiotemporal Independent Component Analysis (EMSICA), is proposed for simultaneously estimating spatiotemporally independent EEG activities and the corresponding cortical source distributions. The proposed approach decomposes the recorded single-trial EEG data into spatiotemporally overlapping components without averaging data from different trials. The cortical source distributions estimated by the approach may be more biologically plausible than the pointwise sources used in equivalent dipole models. The properties of the components (i.e., scalp topographies, ERP image activities, activity spectrums) returned by EMSICA are similar to those returned by the standard ICA in the sense that there is no constraint on spatial orthogonality (as that with PCA), allowing a flexibility in accurately estimating the spatially overlapping projections from functionally separable sources (Makeig et al., 1999). The spatiotemporal framework of EMSICA allows researchers to insert prior knowledge regarding physical source constraints, spatial sparsity, and spatiotemporal independence of the underlying EEG components.

The EMSICA procedure herein described, as applied to EEG data, is verified with stimulus-event-related dynamics collected in a visual 'two-back' continuous performance task. The forward model incorporated a realistic head model using structural magnetic resonance (MR) brain images. Time courses and topographies of several distinctive components will be shown, including those contributing to the late positive complex (LPC) of the target stimulus ERP located in the central parietal, frontal midline, and anterior cingulate cortex, as well as components producing atypical mu rhythms on the precentral gyrus and central posterior alpha activity in the precuneus.

Methods

The spatiotemporal modality

Both theoretical and experimental evidence have shown that scalp-recorded EEG signals are mainly produced by a summand of field activities associated with large cortical pyramidal cells that are typically oriented in parallel perpendicular to the cortical surface. By determining cortical source location and orientation constraints from MR brain images, the orientations of potential sources can be assumed a priori. Consider the time-varying current density $q^{(t)} \in R^J$ distributed at J tessellation elements with fixed orientations in each cell of the volume domain at time t. Associated with each current density contribution is a leadfield matrix $L \in R^{I \times J}$ that contains information about the geometry and conductivity of the model. The data on the I sensors are acquired as

$$x^{(t)} = Lq^{(t)} + \eta^{(t)}, \tag{1}$$

where $\eta^{(t)} \in R^I$ denotes the additive noise assumed to be white and Gaussian which can be removed at the prewhitening stage in applications.

With the known orientation of current density, a spatiotemporal modality can be developed for source imaging based on the cortically constrained, MRI-guided boundary element model. By convention, we also assume that there exist densely distributed sources located in the gray matter. Suppose that the configuration of current density $q^{(t)}$ is constituted by a linear combination of statistically independent time courses or activations $s^{(t)} \in R^K$ that is, $q^{(t)} = Bs^{(t)}$ where $B \in R^{J \times K}$ is a weight matrix with elements b_{jk} that specifies the contribution of the kth source component to the jth tessellation element on the cortex. The kth column of the B matrix specifies the source activation topography on the cortical surface, that is, how much the momentary field configuration varies with the strength of the kth source component $s_k^{(t)}$. We assume numerous spatial source components with different cortical regions whose projections by volume conduction of the scalp surface sum to the I outputs in noiseless mixing

$$x^{(t)} = LBs^{(t)}. \tag{2}$$

In this model, the additive "noise" $\eta^{(t)}$ in Eq. (1) and the artifact signals introduced by eye blinks, eye movements, and other scalp muscle activity are not explicitly modeled, but rather manifested as separate components, (see, e.g., similar treatments in those ICA models by Beckmann et al., 2000; McKeown et al., 1998).

In a Bayesian framework, the inverse problem can be stated as estimating the cortical source distributions as well as their corresponding time courses from given data recorded on the I sensors such that the posterior likelihood of the model

$$p\left(B, s^{(t)} | x^{(t)}, L\right) \propto p\left(x^{(t)} | L, B, s^{(t)}\right) p\left(B, s^{(t)} | L\right) \tag{3}$$

is maximized. The process of extracting the underlying sources can be thought of as producing K spatiotemporal components with

individual spatial distributions (specified as column vectors in B) and time courses at times t (in $s^{(t)}$).

The EMSICA approach

If the cortical activation topographies and temporal magnitude of sources are independently distributed, the prior assumption in Eq. (3) can be reduced to $p(B,s^{(t)}|L) \propto p(B)p(s^{(t)})$. By treating $s^{(t)}$ as nuisance parameters, Eq. (3) can be marginalized into

$$p\left(B|x^{(t)},L\right) \propto p(B)\int ds^{(t)} p\left(x^{(t)}|L,B,s^{(t)}\right)p\left(s^{(t)}\right). \quad (4)$$

Giving the leadfield matrix L, the goal of EMSICA is to find the cortical source topographies, B, for the dependent sensor signals, $x^{(t)}$, that makes the outputs $u^{(t)} \equiv (LB)^{-1}x^{(t)}$ as independent as possible, where $u^{(t)}$ is an estimate of the sources with elements $u_k^{(t)}$ for $k = 1, \ldots, K$. Here, we assume that $I = K$ to guarantee (LB) being a square matrix. A non-square (LB) matrix is discussed in the Discussion section. Because source components are assumed to be independently distributed, the prior $p(u^{(t)})$ can be written as a product of prior probabilities of individual sources, i.e., $p(u^{(t)}) = \prod_k p_k(u_k^{(t)})$. The integral on the right-hand side of Eq. (4) reduces to

$$\frac{1}{det(LB)}\prod_k p_k\left(u_k^{(t)}\right), \quad (5)$$

which is the source likelihood for the observed data likelihood of $x^{(t)}$. The derivation of Eq. (5) is similar to that of the infomax ICA algorithm in a Bayesian framework by several authors (Pearlmutter and Parra, 1996; MacKay, 1996; Knuth, 1997).

We will pay special attention to developing a learning algorithm to recover the cortical activation topographies B using the prior $p(B)$. The elements in the kth column of B can be considered as a realization of the random variable b_k. We assume that those variables are spatially independently distributed with distribution $p_k(b_k)$ such that

$$p(B) = \prod_k p_k(b_k). \quad (6)$$

The prior $p_k(b_k)$ is a probabilistic model that summarizes the spatial properties of an individual source. In conventional minimum-norm inverse models derived from Tikhonov and Arsenin (1977), an individual source is assumed distributed according to a Gaussian prior, an assumption which often produced oversmoothing and, sometimes, unrealistic source configurations. In our method, the prior encompasses both super-Gaussian sources and a powerful class of Gibbs fields (Markov random fields) as follows

$$p_k(b_k) \propto \exp\{-\beta f(b_k)\}\mathrm{sech}^2(b_k), \quad (7)$$

where β is a scalar constant and $f(b_k)$ is a function of the component topography (Chellappa and Jain, 1991). The distribution $p_k(b_k)$ can be seen as measure of sparseness of the kth cortical topography. McKeown et al. (1998) who introduced spatial ICA for fMRI analyses once argued for the sparse nature of spatially distributed patterns in typical cognitive activation paradigms. Some prototypical confounds were also shown to be sparse and localized such as vascular pulsation (i.e., signal localized to larger veins that are moving as a result of cardiac pulsation; see Petersen et al., 2000 for an example). Therefore, imposing a sparse prior is likely well suited for simultaneously source separating and imaging. Elements of b_k, the kth column of B, give the strength of density moments over the cortical surface. Thus, the distribution of b_k must have nonzero strength at few regions and zeros elsewhere. Incorporating this prior information reduces the number of estimated parameters and speeds optimization in the resulting learning algorithm.

In addition to using a sparse prior, the $f(b_k)$ function may be explicitly defined to capture the assumed statistical properties of the spatial source densities. In particular, source current densities may be assumed to be composed of smooth patches possibly separated by discontinuities (Geman and Geman, 1988; Baillet and Garnero, 1997). By taking into account these assumptions, the posterior likelihood becomes

$$p\left(B|x^{(t)},L\right) \sim \prod_k p_k(b_k)\frac{1}{det(LB)}\prod_k p_k\left(u_k^{(t)}\right). \quad (8)$$

In batch learning of the cortical source topographies, B, a small fraction of the data set of block size τ is passed through the learning rule at each iteration. With this in mind, the posterior likelihood must be the product of Eq. (8) over the learning blocks of the data set. Thus, the posterior log-likelihood becomes

$$l = \tau\sum_{j,k}\log\ p_k\left(b_{jk}\right) - \tau\log\ det(LB) + \sum_{k,t}\log\ p_k\left(u_k^{(t)}\right). \quad (9)$$

To find the maximum of this log-likelihood, we take its gradient with respect to B

$$\frac{\partial l}{\partial B} = \tau\phi(B) - \tau L^T(LB)^{-T} - L^T(LB)^{-T}\varphi(U)U^T, \quad (10)$$

where $U = [u^{(1)}, \ldots, u^{(\tau)}]$, $\phi(B) \in R^{J\times K}$, and $\varphi(U) \in R^{K\times\tau}$ are matrices with scores $\phi(b_{jk}) = \partial\log\ p_k(b_{jk})/\partial b_{jk}$ and $\varphi(u_k^{(t)}) = \partial\log\ p_k(u_k^{(t)})/\partial u_k^{(t)}$ respectively. Using the natural gradient technique (Amari, 1998), the resulting gradient decent algorithm can be multiplied by BB^T to avoid computing matrix inversion:

$$\Delta B = B\left[B^T\phi(B) - I - (1/\tau)\varphi(U)U^T\right]. \quad (11)$$

The posterior likelihood in Eq. (8) has spatial and temporal priors in the first and last terms. Note that the spatial term, $B^T\phi(B)$, is symmetrically opposed to the temporal term, $\varphi(U)U^T$.

The cortical map of each EMSICA component may be described as a column in B, that is, b_k containing one value for each tessellation element. Negative values of b_{jk} indicate that the tessellation element is oriented inward to the local orientation of the cortical surface. To find and display vertices strongly active in a particular EMSICA component map, the map values are normalized to z scores for visualization. Dividing the dipole strength estimate for each tessellation element by the standard error of the estimate, we obtain a normalized dipole strength z_{jk} that is t distributed under the null hypothesis of no dipole activity. Regions of activation whose absolute z scores are greater than some threshold (e.g., $|z| > 2.0$ in our empirical study) can be considered strongly active and thus color-coded in the EMSICA component cortical map.

Prewhitening EEG records

Preprocessing EEG signals before statistical analysis or source localization are often a useful step in ERP studies (Baillet et al., 2001b). In ICA applications, the observed data are modeled as $x^{(t)} = W^{-1}s^{(t)}$, where W is a matrix of projection weights and $s^{(t)}$

contains component scores or activations. Observed $x^{(t)}$ are normally preprocessed using the data sphering matrix $\Phi^{-1/2}$ (i.e., $\tilde{x}^{(t)} = \Phi^{-1/2}x^{(t)}$), where Φ is the variance–covariance matrix of the observed data x (Note: The rescaled EEG signals, premultiplied by the estimated W, can be applied directly to obtain the least squares estimate of the component scores, that is, $\hat{s}^{(t)} = \hat{W}\Phi^{-1/2}x^{(t)}$). The data can also be prewhitened by removing machine/physiological artifacts and possible noise, that is, $\tilde{x}^{(t)} = \Lambda^{-1/2}P'x^{(t)}$, where Λ is an $I \times I$ diagonal eigenvalue matrix with only $K < I$ nonzero values in the diagonal and, P, the orthogonal projection matrix (i.e., the eigenvector matrix). Let $\tilde{x}^{(t)}$ be preprocessed data using either $\Phi^{-1/2}$ or $\Lambda^{-1/2}P'$. The model in Eq. (2) can be rewritten as $\tilde{x}^{(t)} = \tilde{L}Bs^{(t)}$, where $\tilde{L} = \Phi^{-1/2}L$ or $\tilde{L} = \Lambda^{-1/2}P'L$. Using prewhitened data allows estimation of a reduced number of spatiotemporal components. The EMSICA learning algorithm in Eq. (11) then can be applied to estimating $B \in R^{J \times K}$ by replacing L with $\tilde{L}$ and $x^{(t)}$ with $\tilde{x}^{(t)}$.

Comparison between ICA and EMSICA

In the standard ICA model, each column of W^{-1} summarizes the relative projection strengths of a source component at the individual EEG scalp sensors. In the EMSICA model, each column of B represents a spatial map describing the topography of synchronous activity on the cortical surface that contributes to the component signal recorded on the scalp. Columns of $A = LB$ give the same information as the W^{-1} matrix in ICA. A detailed comparison between ICA and EMSICA is illustrated in Fig. 1. In applications, we may visualize the cortical source maps, scalp topographies ($A = LB$), and time/frequency plots for the estimated sources when interpreting the functional nature of brain-related sources.

Empirical application of EMSICA

Subjects and cognitive tasks

EMSICA was applied to results of neuropsychological experiment using a 'two-back' visual working memory task. Subjects participated in four N-minute bouts in which a series of single letters A, B, or C were presented at the screen center. Subjects were required to respond whenever a presented letter matched the letter presented just before the preceding stimulus (i.e., the letter 'two-back'). Letter-to-letter stimulus-onset asynchrony was approximately 1816 ms. Subjects were instructed to press either a "Yes" or a "No" key by 934 ms after each letter onset, when an auditory feedback tone was given to indicate whether the answer was right ('beep') or wrong ('buzz').

In each trial, subjects thus had to read the letter presented, decide whether it was identical in name to the letter presented two-back in the sequence, retain the previous one-back letter in memory, and remember the current letter for later comparison (while also 'forgetting' the two-back letter). We recorded EEG and behavioral data (response times and choices) from 71 electrode sites, 69 placed at locations based on a modified International 10–20 System montage, 1 placed below the right eye (VEOG), and 1 placed at the left outer canthus (HEOG). All 71 channels were referred to the right mastoid and were digitally sampled for analysis at 256 Hz with a 0.01 to 100 Hz analog bandpass followed by a 50-Hz low-pass digital filter.

Head and source model

The leadfield matrix L in Eq. (1) was calculated with a four-shell realistic head model using the boundary element method (BEM) (de Munck, 1992; Oostendorp and van Oosterom, 1989). To facilitate recovery of deeper sources, the leadfield was multiplied by a diagonal scaling matrix for column normalization (Pascual-Marqui et al., 1994). It was then necessary to rescale the estimated source contribution matrix B in Eq. (11) afterward. Forward model computation requires knowing the locations of all possible sources, the sensor locations, the compartment boundaries between brain and CSF (likewise, between CSF and skull, skull and scalp, scalp and air), and the relative conductivities of each of the model compartments. We assumed homogeneous isotropic conductivities of 0.33, 1, 0.0042, and 0.33 (Ω^{-1} m^{-1}) for brain, CSF, skull, and scalp, respectively (Mosher et al., 1993).

The four volumes and their boundaries, required for computation of the forward solution, were automatically reconstructed from a high-resolution T1-weighted structural MR image. The compartment boundaries were each represented by 4000 vertices. In our analysis, the solution space of all sources was restricted to be the brain cortex. This improved computational efficiency and reduced the degree of indeterminacy in the inverse problem.

Following segmentation of the cortical surface, the skull, scalp, and cortical surface were tessellated using about 40,000 vertices. In the inverse computation, the solution space comprised approximately 3000 points normal to the local cortical surface, each representing approximately 15 mm^2 (~4 mm × mm) of the cortex. The EEG sensor locations were determined by a fast tracking digitizer (Polhemus, Inc.) which were then coregistered and projected onto the modeled scalp.

The super-Gaussian temporal probability density in Eq. (5) was given by

$$p\left(u_k^{(t)}\right) = g\left(u_k^{(t)}\right)\left[1 - g\left(u_k^{(t)}\right)\right], \tag{12}$$

where $g(u_k^{(t)})$ is the logistic function,

$$g\left(u_k^{(t)}\right) = \frac{1}{1 + \exp\left\{-u_k^{(t)}\right\}}, \tag{13}$$

thus

$$\left(u_k^{(t)}\right) = 1 - 2g\left(u_k^{(t)}\right). \tag{14}$$

The topographic distribution function in Eq. (7) was $f(b_k) = b_k C^{-1} b_k^T$, where $C^{-1} = WW^T$ is the inverse spatial covariance of J tessellation elements. The W matrix computes the first order derivative of the spatial source distribution. Thus

$$\varphi\left(b_{jk}\right) = -2\left[\beta \sum_{j'} r_{jj'} b_{j'k} - \tanh\left(b_{jk}\right)\right], \tag{15}$$

where $r_{jj'}$ denotes jj'th element of C^{-1}.

Results

To evaluate the effectiveness of EMSICA, we compared the dynamic properties of its resulting source components to those obtained by the standard ICA. The data set consisted of 950 concatenated 2.5-s data trials time-locked to letter presentations; EEG records were first decomposed using infomax ICA which

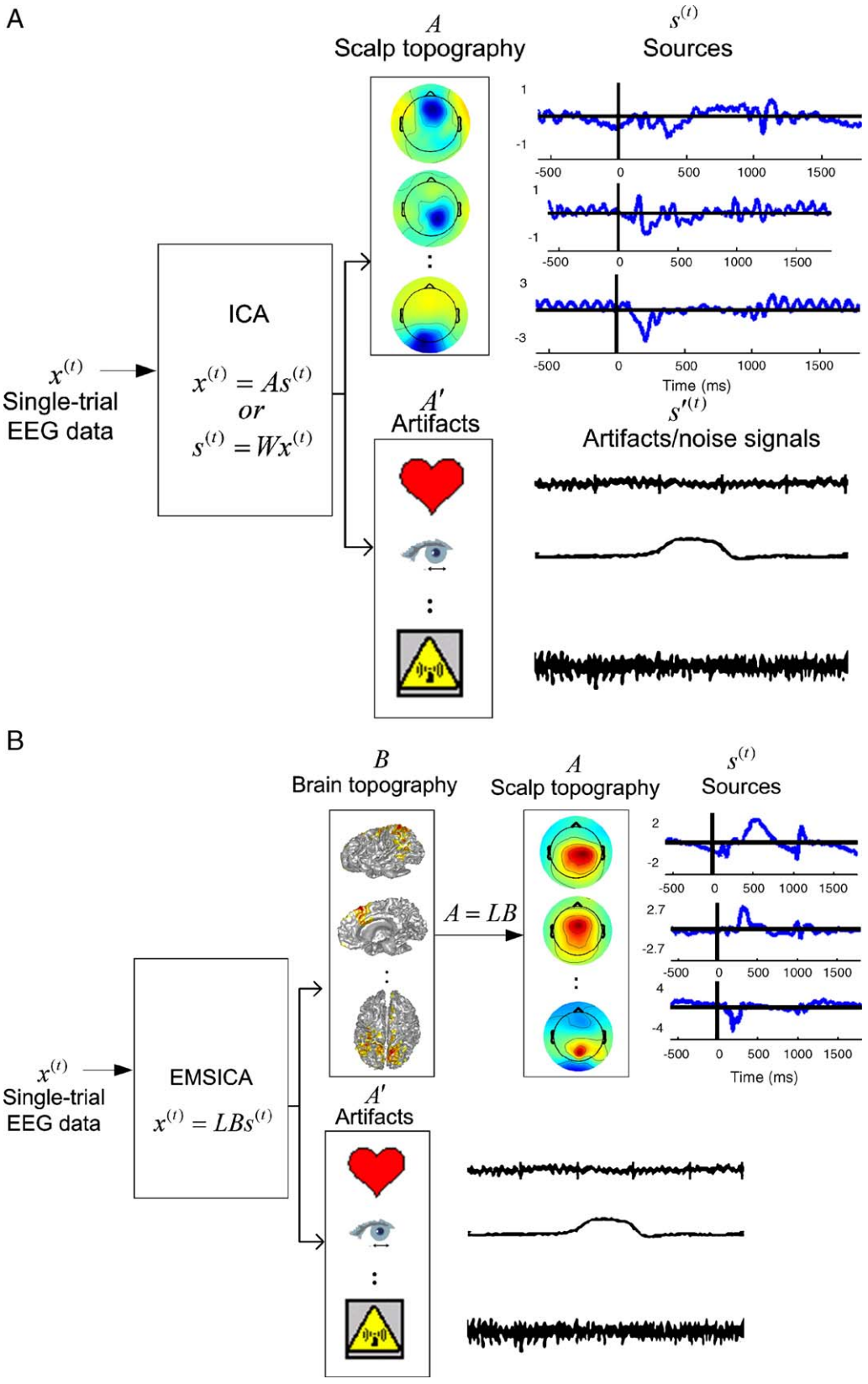

Fig. 1. Comparison of ICA and EMSICA. Infomax ICA (A) finds an un-mixing matrix W that maps the recorded signals to recovered component activities $s^{(t)} = Wx^{(t)}$. Component topographies are read from the columns of the mixing matrix $A = W^{-1}$. These give the projections expected on the scalp if only a single ICA spatiotemporal component was active. Identification of artifact components is possible from distinct properties of these components (Jung et al., 2000). The proposed EMSICA decomposition (B) finds a matrix B of cortical maps using leadfield parameters that give their projections to the scalp sensors using a biophysical model, $s^{(t)} = LBx^{(t)}$. Thus, EMSICA separates EEG features into activities of fixed cortical maps rather than as activities of fixed scalp maps.

exploited temporal independence for blind source separation. After training, the resulting 71 components were ranked by amount of total EEG variance accounted for and the twelve largest components were selected for display in Fig. 2A. Next, the same data set was analyzed by EMSICA. Ten of the 12 ICA components turned out to have time courses and scalp projections similar to EMSICA components including those producing major parts of the P300 or LPC feature of the average evoked response as well as components accounting for somatomotor mu, frontal midline theta, and central and lateral posterior alpha rhythms. The dynamic properties of four nonartifact components are visualized in Figs. 3–6, each of which shows the scalp map, activity ERP image plot,

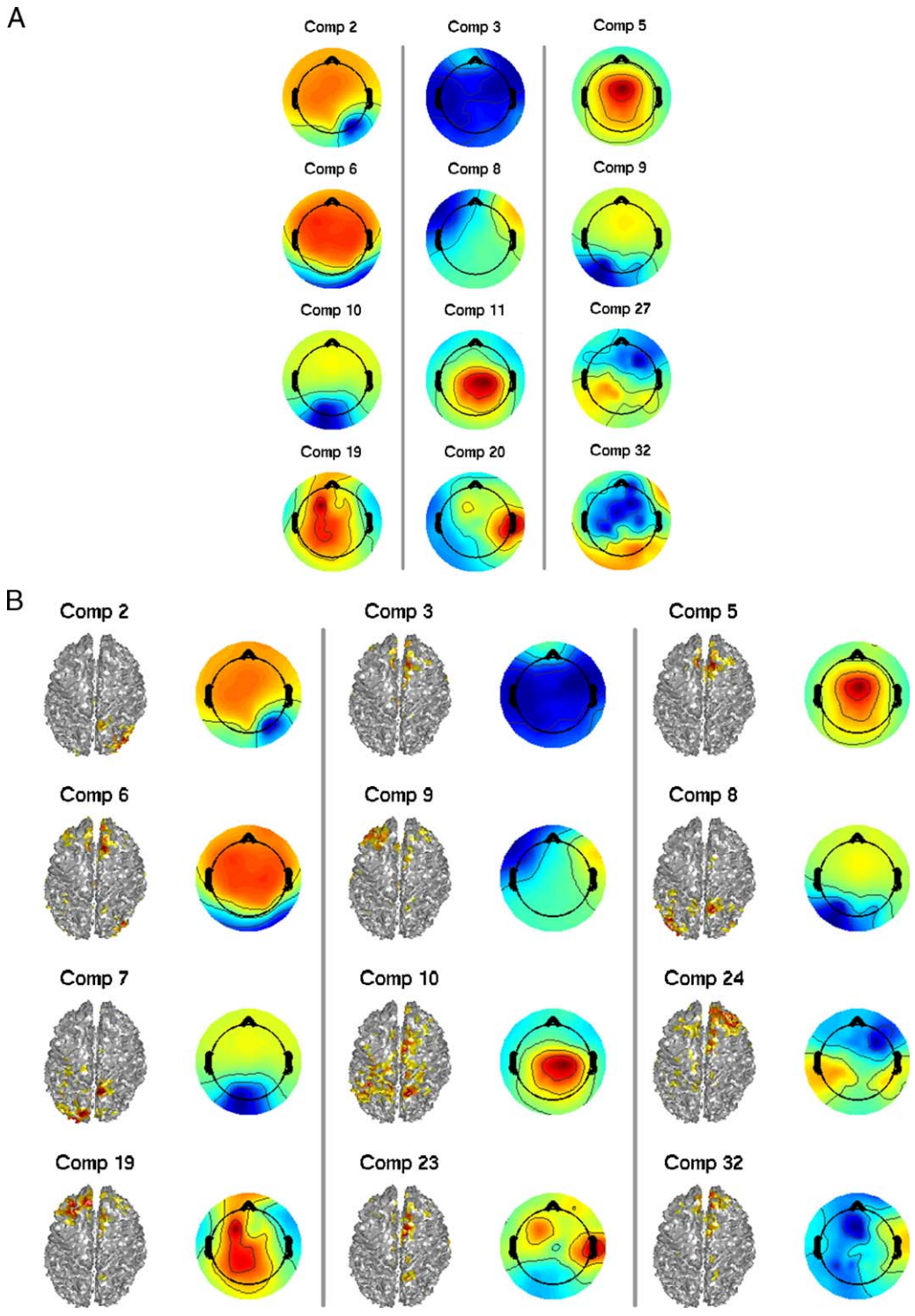

Fig. 2. Maps of strong component pairs estimated using ICA and EMSICA. (A) Scalp maps of 12 strong and near-dipolar infomax ICA components. (B) Ten corresponding components found by EMSICA. Left columns show the component cortical activation topographies obtained by EMSICA, right panels show their projections to the scalp sensors.

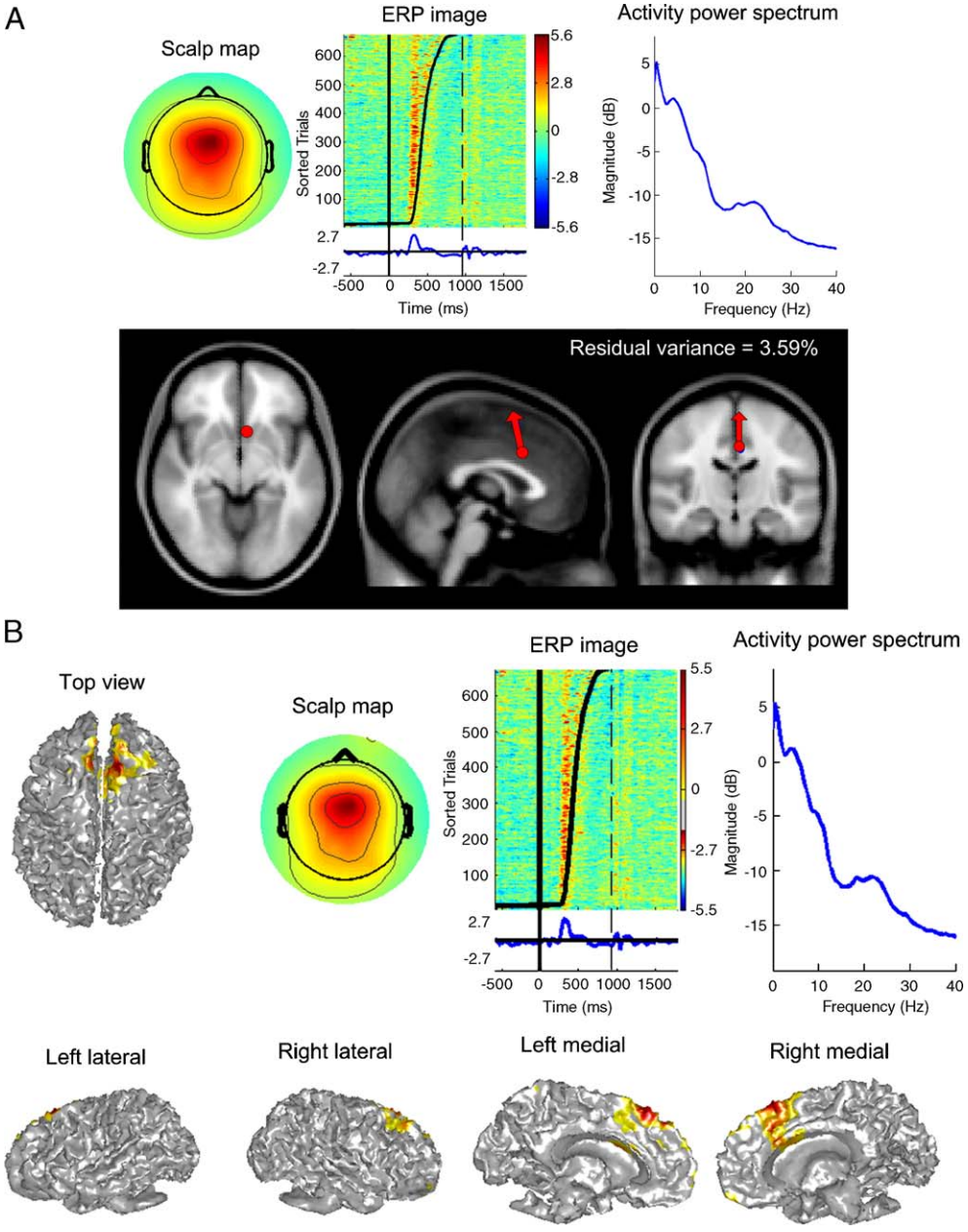

Fig. 3. A matching pair of ICA and EMSICA components projecting to the frontal midline, anterior cingulate, and premotor cortex. (A) From infomax ICA; (B) from EMSICA. Both show a premotor theta response pattern. Upper row: left panels show the component scalp topographies; middle images, the ERP image activity plots; right panels, frequency spectra. In the ERP image plots, color lines for individual trials are stacked on top of each other. The individual trials are time-locked to the response (solid vertical line) and sorted by RT from stimulus onset (solid curve). The dashed vertical line denotes 934 ms after each letter onset when an auditory feedback tone was given. The mean ERP component time course is shown beneath the ERP image. Readers are referred to Makeig et al. (1999) and Jung et al. (2000) for more details. The lower row of the panel A shows single equivalent current dipole location for this ICA component, estimated from the scalp map (upper left) and plotted on a mean MRI image (Montreal Neurological Institute) from three different perspectives (axial, sagittal, and coronal views). The low residual variance (r.v.) for the dipole fit is shown. In the upper left panel and lower panels of B, the active region of the corresponding EMSICA component cortical map is shown. Activation with a z score of 2 or greater is indexed by the color code. For ICA, component scalp maps are input into a source localization algorithm to estimate their equivalent dipole location. For EMSICA, the cortical distributed source image and the spatiotemporal separation are computed simultaneously.

and activity spectrum associated with components. The lower row of each figure shows the best-fitting single equivalent current dipole location plus scalp and cortical maps for the ICA and EMSICA components, respectively. Dipole locations were estimated by submitting the corresponding column in the inverse matrix obtained from infomax ICA to an automatic one or dual-symmetric dipole source localization algorithm (DIPFIT, contributed by R. Oostenveld et al.) as was implemented in EEGLAB (Delorme and Makeig, 2004); the dipole model was implemented using a standard four-shell spherical head model with radii of 71, 72, 79, and 85 mm and the same source model conductivities used in EMSICA. The residual variance (r.v.) (i.e., the amount of

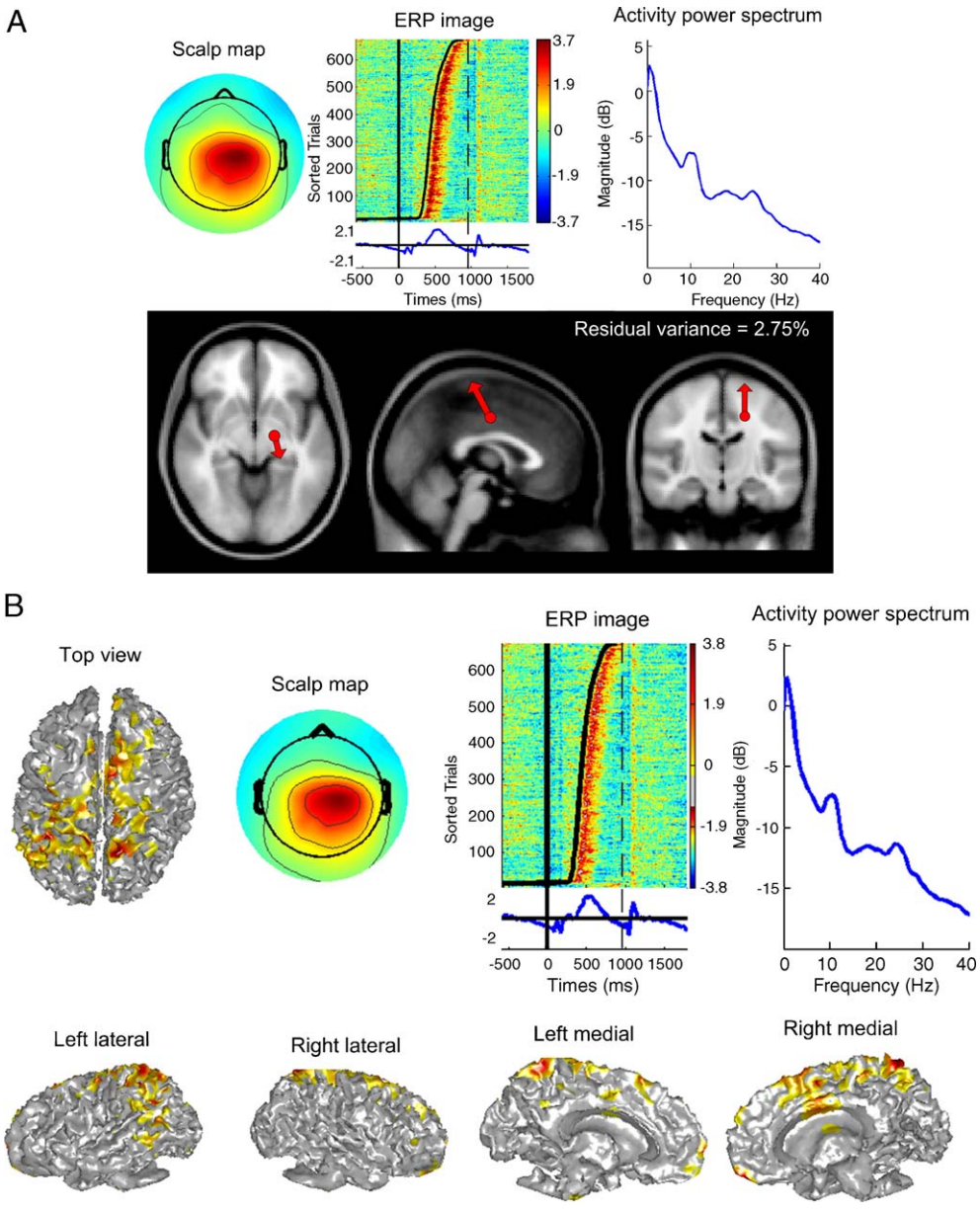

Fig. 4. Independent components contributing to the post-response (P3b) positivity, located to central parietal and right frontal lobe by ICA (A) and EMSICA (B), respectively. Panels as in Fig. 3. Frontal midline components often exhibit a 4–8 Hz theta band peak in their activity spectra during tasks requiring concentration.

residual variance in the component scalp map or sensor space projection) not accounted for by the dipole model is shown on the upper right corner of each dipole model panel.

The top left and lower panels of Figs. 3B–6B show EMSICA component cortical maps found by assuming that a spatiotemporal independent component accounts for synchronous activity within a connected cortical domain. Conditions that require mental concentration often induce midfrontal theta bursts in the EEG (Mizuki et al., 1980; Gevins et al., 1997; Uchida et al., 2003; Onton et al., 2005). The region is implicated by fMRI and neurophysiological experiments as performance monitoring system, signaling the need for a behavioral change to optimize action outcome (Ullsperger and von Cramon, 2003; Rushworth et al., 2004). As shown in Fig. 3B, EMSICA placed the principal cortical generator of the frontal midline theta around the dorsal anterior cingulate, though the cortical model was possibly not fine enough to model activity within the anterior cingulate gyrus itself.

The EMSICA component in Fig. 4B has a central parietal maximum and a right-scalp bias and makes a substantial contribution to the slow postmotor P300 or P3b positivity following target presentations. The P3b component is an endogenous, positive polarity component of the human ERP (Fabiani et al., 1987) that occurred in this experiment a moment after the motor command.

Fig. 5 shows an atypical left mu rhythm component (not exhibiting the usual near 10-Hz/20-Hz spectral peak) located, in the EMSICA model, over hand motor cortex and adjacent postcentral somatosensory areas. The near 20-Hz peak in the component power spectrum was strongly blocked following movements (not shown). Before and after the button press, the

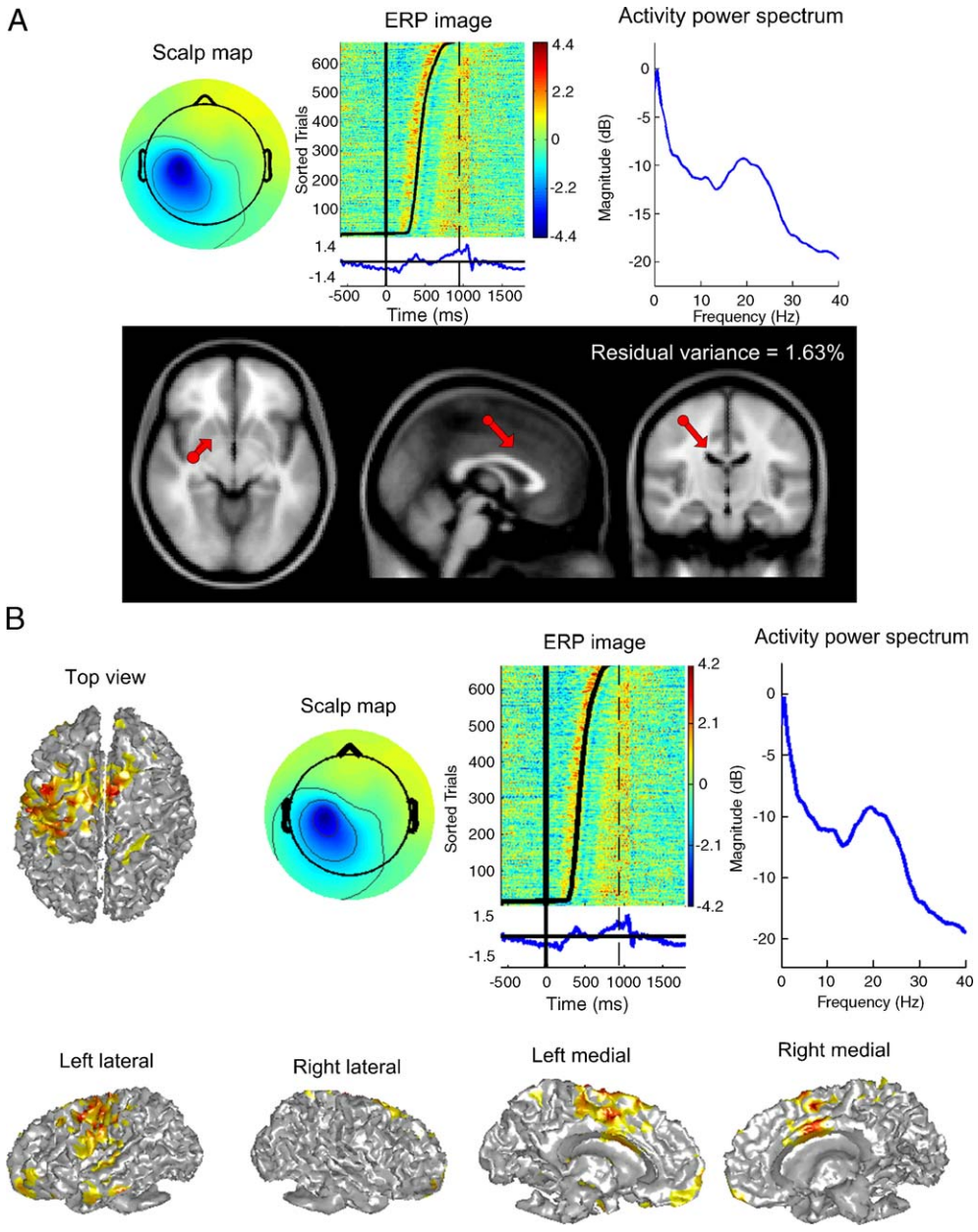

Fig. 5. Corresponding independent component processes found by ICA (A) and EMSICA (B), showing a polarity change above motor cortex on the left side of the brain and an atypical broad 20-Hz spectral peak. Panels as in Fig. 3. The EMSICA component is active near hand premotor cortex and in the adjacent precentral gyrus.

component produces a brief theta band oscillation loosely time-locked to the motor response (Makeig et al., 2004).

The prevailing topographies of alpha sources in this subject can be seen in components 7, 8, and 9 in Fig. 2B. While multiple alpha rhythms are separated by ICA (Makeig et al., 2002 and Fig. 2A), EMSICA here separated their activities and identified their partly, spatially overlapping cortical topographies based on the relative spatiotemporal independence of their activity patterns in the unaveraged data. Fig. 6 shows a posterior alpha component with a distinct spectral peak near 10 Hz that is synchronously active across areas in both hemispheres (possibly densely connected via corpus callosum). Here, both single and bilateral equivalent current dipole models of the corresponding ICA component (A) have residual variances larger than 10%.

Discussion

A spatiotemporal ICA model proposed recently made similar independence assumptions on the mixing matrix and time components (stICA, Stone et al., 2002). It performs ICA both in the temporal and spatial domain as defined by the mixing matrix. However, this spatiotemporal ICA method used PCA to first decompose the data set into spatial eigenimages and temporal eigensequences. That is, given the first eigendecomposition on the data set $X = QDV' = (QD^{1/2})(D^{1/2}V') = \tilde{Q}\tilde{V}'$ where X is the data matrix with the I sensors by total number of data points in the time sequence; Q is an $I \times K$ matrix of K eigenimages with $K \leq I$; V is a matrix of K eigensequences; likewise, D is a diagonal matrix of its eigenvalues. The stICA approach embodies the assumption that

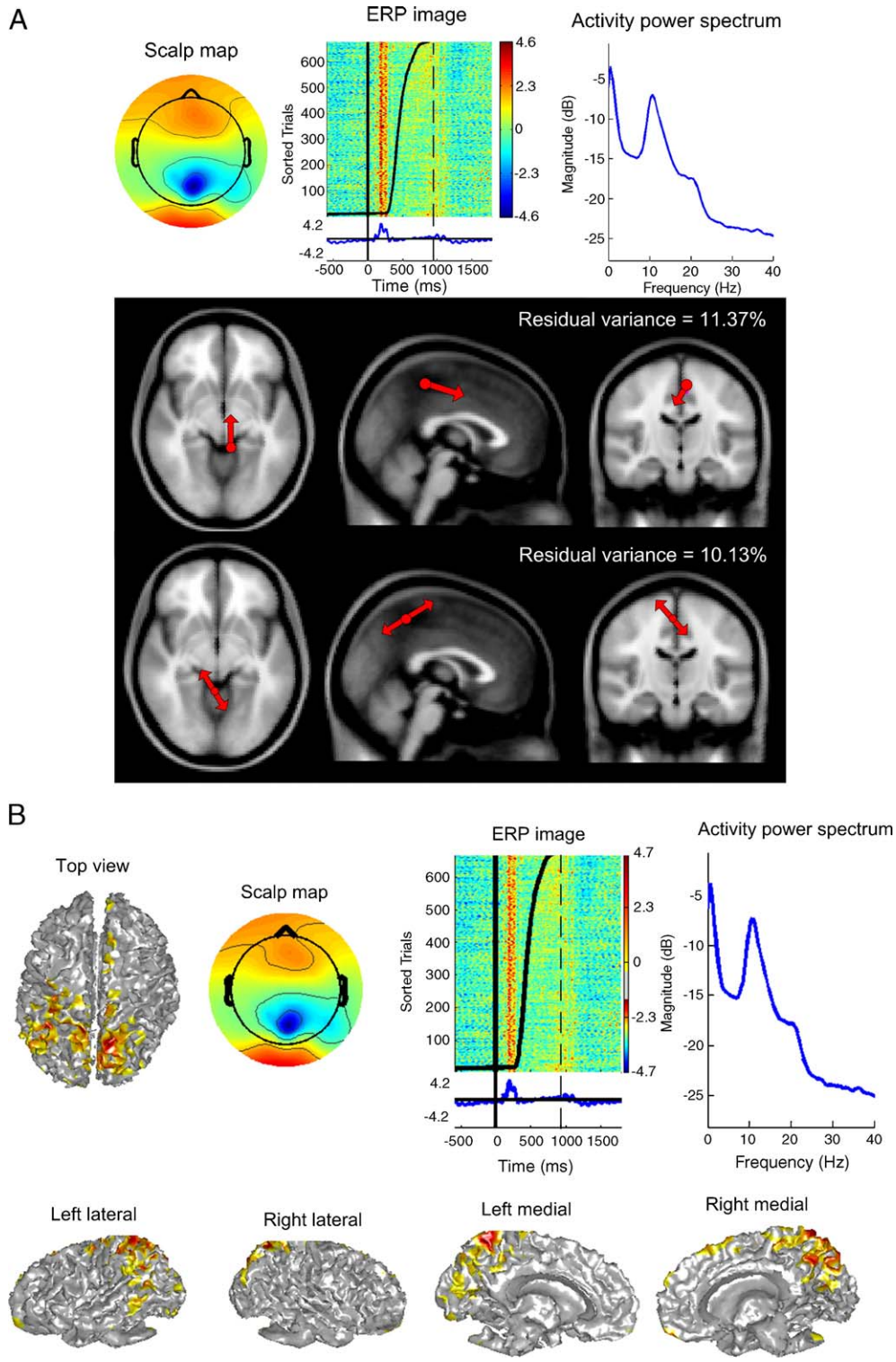

Fig. 6. Corresponding central posterior alpha components retrieved by ICA (A) and EMSICA (B) exhibiting a pattern of prolonged partial phase resetting following auditory feedback (see ERP images, right vertical lines). The lower panel of A shows best-fitting single and bilateral equivalent current dipole models, estimated from the ICA scalp map, that reveal possible difficulty of always characterizing ICA components as the projection of a single (or/and bilateral) equivalent current dipole model. Here, residual variances of both single- and dual-dipole models were larger than 10%, and the corresponding EMSICA component had a more complex active region.

each eigenimage in $\tilde{Q}$ is a linear combination of K spatially independent images, and each eigensequence in $\tilde{V}$ is a linear combination of K temporally independent sequences. The infomax criterion is then applied to the eigenimages and eigensequences. The EMSICA approach, on the other hand, does not depend on the PCA-like method to decompose data sets. In a Bayesian

framework, it yet permits a trade-off between a dual independence: one for cortical source topographies and the other for source activity time courses (the first and last terms in Eq. (11)).

Since high temporal resolution is the main advantage of EEG and MEG imaging, use of information contained in those unaveraged data can bring crucial help to source reconstruction methods. The EMSICA algorithm fully uses information distributed throughout the entire EEG (or MEG) signals to separate and to image cortical sources. However, it is important to point out some remaining practical issues and questions. First, the use of an approximate biophysical forward model derived from the MR image adds a possible source of error to the infomax procedure. Second, the effects of altering the algorithmic parameters, for example, β and $f(b_k)$ in Eq. (7), need to be carefully examined since the exact choice of the nonlinear form of the temporal and spatial prior, $p(s^{(t)})$ and $p(B)$, respectively, may have considerable and unknown consequences. During the time course of an experiment, various artifact signals are introduced into the recorded data such as eye blinks, eye movements, and other scalp muscle activities. As shown in Fig. 1, EMSICA makes an explicit assumption that there exist latent parameters, $B_{\text{artifacts}}$, in the cortical domain B, such that artifact scalp topographies can be recovered as $A_{\text{artifacts}} = LB_{\text{artifacts}}$. Although this may be reasonable from the mathematical point of view, it is likely that an individualized volume conductor model containing additional relevant compartments (i.e., eyeballs and head muscles) would provide additional information for artifact separation and identification. On the other hand, EMSICA might be applied to the data subspace remaining after artifacts of non-cortical region, identified by PCA or ICA, are first removed from the data.

When deriving the EMSICA approach, we assumed that $I = K$ to guarantee (LB) being a square matrix and sources can be likewise estimated by $u^{(t)} \equiv (LB)^{-1}x^{(t)}$. For a rectangular mixing matrix, a possible approach for estimating sources can be implemented by maximizing a posteriori value of $u^{(t)}$ for $\hat{u}^{(t)} = \max_{u^{(t)}} p\left(u^{(t)}|x^{(t)}, LB\right)$ (e.g., see Lee et al., 1999 in details).

It is possible that Monte Carlo modeling studies (Liu et al., 1998), sampling over numerous possible source locations, sizes, and orientations could be used to determine the theoretical and/or effective limits of EMSICA accuracy. Also decomposing more data sets, followed by advanced cortical activation component clustering methods applied to decompositions from more subjects, might allow further validation of the effectiveness of the proposed method.

Conclusion

In this paper, an EMSICA decomposition using explicit and implicit constraints (cortically constrained and spatiotemporally independent sources with sparse priors) is proposed to attack the indeterminate nature of the EEG source analysis problem. The proposed method aims to separate the recorded mixture of EEG features and artifacts into neurophysiologically and neuroanatomically meaningful components within a simple systematic learning framework.

The Bayesian framework allows researchers to introduce a priori information as to the possible locations of the generating source domains by locally defining topography of relative dipole strengths, which depend on discontinuity priors in cortical activation topography according to anatomical and physiological knowledge. If one had knowledge of the correlation of activity between different sources, such information could be incorporated to allow the imposition of a smoothness constraint on the inverse solution, as in the LORETA approach (Pascual-Marqui et al., 1994). In EMSICA, the magnitudes of the current in each component are assumed to have a super-Gaussian instead of a Gaussian distribution to address issues with spatially oversmoothing and most likely unrealistic source configurations found by the conventional minimum-norm approach.

The proposed method can be seen as an extension of conventional infomax or maximum likelihood ICA. Compared to PCA-like processing, EMSICA removes the constraint of orthogonality and forces components to be approximately independent rather than simply uncorrelated. The estimated components may potentially reflect accurately the spatially overlapping sources. Prior knowledge of the leadfield matrix, sparseness of source distributions, and spatiotemporal independence are imposed in the Bayesian framework, permitting a trade-off between prior knowledge, mutual independence of spatial cortical maps, and mutual independence of their corresponding time courses. While ICA finds an un-mixing matrix that represents the component scalp topographies, EMSICA finds a matrix of spatial maps that describe the component regions of partially synchronous local field activity on the modeled cortical surface. Both methods extract the dynamics of macroscopic neuronal activities in the brain by analyzing collections of unaveraged event-related EEG epochs, thus revealing more information about event-related brain dynamics than is likely obtainable from post-processing of simple response averages.

The next step in this investigation will be to examine between-subject spatiotemporal component stability by clustering EMSICA components with similar activation power spectra and cortical activation topographies. Recently, researchers have introduced the dynamics of brain activation and synchronization phenomena with high temporal resolution through ICA (Delorme et al., 2002). It would also be interesting to investigate into repulsively coupled clusters and those research findings on different ensembles of brain sources coherent over short time intervals in an oscillatory fashion proposed by Tass and Haken (1996) and Tass (1999). The proposed EMSICA makes it possible to study event-related dynamics as well as their time-varying coherence of these independent EEG sources directly on brain topographies following the stimulus onset.

Acknowledgments

This research was supported by grants NSC92-2413-H-001-005 and NSC94-2413-H-001-003 from the National Science Council, Taiwan, by the National Institutes of Health USA (RO1-MH/RR61619-01 and RO1-NS047293), and by the Swartz foundation (Stony Brook, NY).

References

Amari, S., 1998. Natural gradient works efficiently in learning. Neural Comput. 10 (2), 251–276.

Andrew, C., Pfurtscheller, G., 1997. On the existence of deferent alpha band rhythms in the hand area of man. Neurosci. Lett. 222, 103–106.

Baillet, S., Garnero, L., 1997. A Bayesian approach to introducing anatomo-functional priors in the EEG/MEG inverse problem. IEEE Trans. Biomed. Eng. 44 (5), 374–385.

Baillet, S., Mosher, J.C., Leahy, R.M., 2001a. Electromagnetic brain mapping. IEEE Trans. Signal Process. Mag., 14–30.

Baillet, S., Riera, J.J., Marin, G., Mangin, J.F., Aubert, J., Garnero, L., 2001b. Evaluation of inverse methods and head models for EEG source localization using a human skull phantom. Phys. Med. Biol. 46 (1), 77–96.

Beckmann, C.F., Noble, J.A., Smith, S.M., 2000. Artefact detection in fMRI data using independent component analysis. NeuroImage 11, S614.

Cao, J., Murata, N., Amari, S., Cichocki, A., Takeda, T., 2001. A robust ICA approach for unaveraged single-trial auditory evoked fields data decomposition. 3rd International Conference on Independent Component Analysis and Signal Separation, pp. 445–450.

Chellappa, R., Jain, A., 1991. Markov Random Fields: Theory and Applications. Academic Press, San Diego.

Dale, A.M., Sereno, M.I., 1993. Improved localization of cortical activity by combining EEG and MEG with MRI cortical surface reconstruction: a linear approach. J. Cogn. Neurosci. 5, 162–176.

Delorme, A., Makeig, S., 2004. EEGLAB: an open source toolbox for analysis of single-trial EEG dynamics including independent component analysis. J. Neurosci. Methods 134, 9–21.

Delorme, A., Makeig, S., Fabre-Thorpe, M., Sejnowski, T.J., 2002. From single-trial EEG to brain area dynamics. Neurocomputing 44–46, 1057–1064.

de Munck, J.C., 1992. A linear discretization of the volume conductor boundary integral equation using analytically integrated elements. IEEE Trans. Biomed. Eng. 39, 986–990.

Fabiani, M., Gratton, G., Karis, D., Donchin, E., 1987. The definition, identification and reliability of measurement of the P300 component of the event-related brain potential. In: Ackles, P.K., Jennings, J.R., Coles, M.G. (Eds.), Adv. Psychophysiol., vol. 2. JAI Press, Greenwhich, CT, pp. 1–78.

Fuchs, M., Wagner, M., Kohler, T., Wischmann, H.A., 1999. Linear and nonlinear current density reconstructions. J. Clin. Neurophysiol. 6 (7), 67–295.

Geman, S., Geman, D., 1988. Stochastic relaxation, Gibbs distributions, and the Bayesian restoration of images. IEEE Trans. Pattern Anal. Machine Intell. 6, 721–741.

Gevins, A., Smith, M.E., McEvoy, L., Yu, D., 1997. High-resolution EEG mapping of cortical activation related to working memory: effects of task difficulty, type of processing, and practice. Cereb. Cortex 7, 374–385.

Halgren, E., Dhond, R.P., Christensen, N., Petten, C.V., Marinkovic, K., Lewine, J.D., Dale, A.M., 2002. N400-like magnetoencephalography responses modulated by semantic context, word frequency, and lexical class in sentences. NeuroImage 17, 1101–1116.

Hämäläinen, M.S., Ilmoniemi, R.J., 1984. Interpreting measured magnetic fields of the brain: estimates of current distributions. Helsinki Univ Tech Rep. TKK-F-A559.

Hämäläinen, M.S., Ilmoniemi, R.J., 1994. Interpreting magnetic fields of the brain: minimum norm estimates. Med. Biol. Eng., 32.

Jung, T.P., Makeig, S., Humphries, C., Lee, T.W., McKeown, M.J., Iragui, V., Sejnowski, T.J., 2000. Removing electroencephalographic artifacts by blind source separation. Psychophysiology 37, 163–178.

Jung, T.P., Makeig, S., Mckeown, M.J., Bell, A.J., Lee, T.W., Sejnowski, T.J., 2001. Imaging brain dynamics using independent component analysis. Proc. IEEE 89 (7), 1107–1122.

Kincses, W., Braun, C., Kaiser, S., Elbert, T., 1999. Modeling extended sources of event-related potentials using anatomical and physiological constraints. Hum. Brain Mapp. 8, 182–193.

Knuth, K.H., 1997. Difficulties applying recent blind source separation techniques to EEG and MEG. In: Boise 1998, Erickson, G.J. (Eds.), Maximum Entropy and Bayesian Methods. Kluwer Academic, Dordrecht: Kluwer, Academic Publishers, pp. 209–222.

Lee, T.W., Lewicki, M.S., Girolami, M., Sejnowski, T.J., 1999. Blind source separation of more sources than mixtures using overcomplete representations. IEEE Signal Process. Lett. 6 (4), 87–90.

Liu, A.K., Belliveau, J.W., Dale, A.M., 1998. Spatiotemporal imaging of human brain activity using fMRI constrained MEG data: Monte Carlo simulations. Proc. Natl. Acad. Sci. U. S. A. 95, 8945–8950.

Liu, Y., Perfetti, C., Hart, L., 2003. ERP evidence for the time course of graphic, phonological, and semantic information in Chinese meaning and pronunciation decisions. J. Exp. Psychol.: Learn. Mem. Cogn. 29, 1231–1247.

Lutzenberger, W., 1997. EEG alpha dynamics as viewed from EEG dimension dynamics. Int. J. Psychophysiol. 26 (1–3), 273–283.

MacKay, D., 1996. Maximum likelihood and covariant algorithms for independent component analysis. http://www.wol.ra.phy.cam.ac.uk/mackay/.

Makeig, S., Bell, A.J., Jung, T.P., Sejnowski, T.J., 1996. Independent component analysis of electroencephalographic data. Adv. Neural Inf. Process. Syst. 8, 145–151.

Makeig, S., Westerfield, M., Jung, T., Covington, J., Townsend, J., Sejnowski, T., Courchsne, E., 1999. Functionally independent components of the late positive event-related potential during visual spatial attention. J. Neurosci. 19 (7), 2665–2680.

Makeig, S., Westerfield, M., Jung, T., Enghoff, S., Townsend, J., Courchesne, E., Sejnowski, T., 2002. Dynamic brain sources of visual evoked responses. Science 295, 690–694.

Makeig, S., Delorme, A., Westerfield, M., Townsend, J., Courchense, E., Sejnowski, T., 2004. Electroencephalographic brain dynamics following manually responded visual targets. PLOS Biol. 2, 747–762.

Mangun, R., 1992. In: Basar, E., Bullock, T.H. (Eds.), Induced Rhythms in the BrainBirkhäuser, Boston.

McKeown, M.J., Makeig, S., Brown, G.G., Jung, T.P., Kindermann, S.S., Bell, A.J., Sejnowski, T.J., 1998. Analysis of FMRI data by blind separation into independent spatial components. Brain Mapp. 6, 160–188.

Mizuki, Y., Tanaka, M., Isozaki, H., Nishijima, H., Inanaga, K., 1980. Periodic appearance of theta rhythm in the frontal midline area during performance of a mental task. Electroencephalogr. Clin. Neurophysiol. 49, 345–351.

Moores, K.A., Clark, C.R., Hadfield, J.L., Brown, G.C., Taylor, D.J., Fitzgibbon, S.P., Lewis, A.C., Weber, D.L., Greenblatt, R., 2003. Investigating the generators of the scalp recorded visuo-verbal p300 using cortically constrained source localization. Hum. Brain Mapp. 18, 53–77.

Mosher, J., Leahy, R., 1998. Recursive MUSIC: a framework for EEG and MEG source localization. IEEE Trans. Biomed. Eng. 45, 1342–1354.

Mosher, J., Lewis, P., Leahy, R., 1992. Multiple dipole modeling and localization from spatio-temporal MEG data. IEEE Trans. Biomed. Eng. 39, 541–557.

Mosher, J.C., Spencer, M.E., Leahy, R.M., Lewis, P.S., 1993. Error bounds for MEG and EEG dipole source localization. Electroencephalogr. Clin. Neurophysiol. 86, 303–321.

Nunez, P.L., Pilgreen, K.L., Westdorp, A.F., Law, S.K., Nelson, A.V., 1991. A visual study of surface potentials and laplacians due to distributed neocortical sources: computer simulated and evoked potentials. Brain Topogr. 4, 151–168.

Nunez, P.L., Silberstein, R.B., Cadusch, P.J., Wijesinghe, R.S., Westdorp, A.F., Srinivasan, R., 1994. A theoretical and experimental study of high resolution EEG based on surface laplacians and cortical imaging. Electroencephalogr. Clin. Neurophysiol. 90, 40–57.

Onton, J., Delorme, A., Makeig, S., 2005. Frontal midline EEG dynamics during working memory. NeuroImage 27, 341–356.

Oostendorp, T.F., van Oosterom, A., 1989. Source parameter estimation in inhomogeneous volume conductors of arbitrary shape. IEEE Trans. Biomed. Eng. 36, 382–391.

Pascual-Marqui, R.D., Michel, C.M., Lehmann, D., 1994. Low resolution electromagnetic tomography: a new method for localizing electrical activity of the brain. Int. J. Psychophysiol. 18, 49–65.

Pearlmutter, B.A., Parra, L.C., 1996. A context-sensitive generalization of ICA, 1996. International Conference on Neural Information Processing, Hong Kong.

Petersen, K.S., Hansen, L.K., Kolenda, T., Rostrup, E., Strother, S.C., 2000. On the independent components of functional neuroimages. Proc. Int.

Conf. on Independent Component Analysis and Blind Signal Separation, Helsinki, pp. 615–620.
Rushworth, M.F., Walton, M.E., Kennerley, S.W., Bannerman, D.M., 2004. Action sets and decisions in the medial frontal cortex. Trends Cogn. Sci. 8 (9), 410–417.
Scherg, M., Cramon, D.V., 1985. Two bilateral sources of the late AEP as identified by a spatio-temporal dipole model. Electroencephalogr. Clin. Neurophysiol. 62, 32–44.
Scherg, M., Cramon, D.V., 1986. Evoked dipole source potentials of the human auditory cortex. Electroencephalogr. Clin. Neurophysiol. 65, 344–360.
Schmidt, D.M., George, J.S., Wood, C.C., 1999. Bayesian inference applied to the electromagnetic inverse problem. Hum. Brain Mapp. 7, 195–212.
Spencer, K.M., Dien, J., Donchin, E., 2001. Spatiotemporal analysis of the late ERP responses to deviant stimuli, psychophysiology. Psychophysiology 38, 343–358.
Stone, J.V., Porrill, J., Porter, N.R., Wilkinson, I.W., 2002. Spatiotemporal independent component analysis of event-related fMRI data using skewed probability density functions. NeuroImage 15 (2), 407–421.
Tang, A.C., Phung, D., Pearlmutter, B.A., Christner, R., 2000. Localization of independent components from magnetoencephalography. Workshop on Independent Component Analysis and Blind Signal Separation, pp. 387–392.
Tass, P.A., 1999. Phase Resetting in Medicine and Biology—Stochastic Modelling and Data Analysis. Springer, Berlin.
Tass, P., Haken, H., 1996. Synchronized oscillations in the visual cortex—A synergetic model. Biol. Cybern. 74, 31–39.
Tendolkar, I., Rugg, M.D., Fell, J., Vogt, H., Scholz, M., Hinrichs, H., Heinze, H.J., 2000. A magnetoencephalographic study of brain activity related to recognition memory in healthy young human subjects. Neurosci. Lett. 280, 69–72.
Tikhonov, A., Arsenin, V., 1977. Solutions of Ill-Posed Problems. Winston, Washington, DC.
Uchida, S., Maehara, T., Hirai, N., Kawa, K., Shimizu, H., 2003. Theta oscillation in the anterior cingulate and beta-1 oscillation in the medial temporal cortices: a human case report. J. Clin. Neurosci. 10 (3), 371–374.
Ullsperger, M., von Cramon, D.Y., 2003. Error monitoring using external feedback: specific roles of the habenular complex, the reward system, and the cingulate motor area revealed by fMRI. J. Neurosci. 23 (10), 4308–4314.
Vigário, R., Särelä, J., Jousmaki, V., Oja, E., 1999. Independent component analysis in decomposition of auditory and somatosensory evoked fields. First International Conference on Independent Component Analysis and Signal Separation, pp. 167–172.
Zhukov, L.E., Weinstein, D.W., Johnson, C., 2000. Independent component analysis for EEG source localization in realistic head models. IEEE Eng. Med. Biol. 19, 87–96.